IEEE Access
Multidisciplinary | Rapid Review | Open Access Journal

Received March 29, 2022, accepted April 7, 2022, date of publication April 13, 2022, date of current version April 20, 2022.

Digital Object Identifier 10.1109/ACCESS.2022.3167148

Optimization and Performance Evaluation of Non-Overlap Wound-Field Converter-Fed and Direct-Grid Wind Generators

KAREN S. GARNER[1], (Member, IEEE), UDOCHUKWU B. AKURU[2], (Senior Member, IEEE), AND MAARTEN J. KAMPER[3], (Senior Member, IEEE)

[1]Electrical and Electronic Engineering Department, Stellenbosch University, Stellenbosch 7600, South Africa
[2]Department of Electrical Engineering, Tshwane University of Technology, Pretoria 0183, South Africa
[3]Electrical Engineering Department, Stellenbosch University, Stellenbosch 7600, South Africa

Corresponding author: Karen S. Garner (garnerks@sun.ac.za)

This work was supported in part by the National Research Foundation under Grant NFSG180517331203.

ABSTRACT Non-overlap winding technology continues to remain relevant in the design of wound-field machines as an alternative for high torque density permanent magnet machines. In this paper, the finite element analyses-optimisation of two variants of the non-overlap wound-field machines viz., wound-field flux switching machine (WF-FSM) and phase shifting wound rotor synchronous machine (WRSM), are compared, first in terms of their performance for large-scale converter-fed wind generator drives, then experimentally as sub-scaled converter-fed versus direct grid-connected wind generators, respectively. This study is unique because there are no prior attempts to design, optimize and analyse on these machines for medium-speed wind power generation, as well as experiment on sub-scale prototypes for direct-grid and converter-fed operation. All investigations are contemplated in the medium-speed wind generator drivetrain which provides a tradeoff for generator efficiency and size. From the global optimisation of both machines at large-scale power levels, the torque per mass of the WF-FSM is found to be 50 % lesser compared to the WRSM. This is due to approximate volume, with closely matched optimal split and aspect ratios. In terms of the sub-scaled experimentation, both generators can easily vary their generated output power to match with varying wind resource, but direct grid-connected WRSM generator yields better efficiency performance compared to the WF-FSM converter-fed operating mode, given that the generator terminal voltage of the former is highly regulated.

INDEX TERMS Converter-fed, direct grid-connected, finite element analyses, non-overlap winding, optimization, medium-speed wind generators, wound-field flux switching machine (WF-FSM), wound rotor synchronous machine (WRSM).

I. INTRODUCTION

Wind power capacity grew by a record additional capacity of 93 GW in 2020, with most of the new generation coming from onshore installation [1]. The cost of wind power generation is decreasing to the point that wind energy is becoming more competitive with fossil fuel generation. Offshore wind installations are designed with very large turbines, usually with power capacity more than 5 MW, as well as futuristic concepts of up to 20 MW [2], [3]. Onshore wind generators are typically in the 0.5 to 3 MW range.

The associate editor coordinating the review of this manuscript and approving it for publication was Kan Liu.

High-speed (above 600 r/min) geared wind generators, because of their small size and low weight, have dominated the wind industry, but the drawback of these generators is the complex gearbox design that requires three stages [4]. Low-speed (below 100 r/min) wind generators do not require a gearbox, but these machines become very large, heavy and costly [5], [6]. Medium-speed (100-500 r/min) solutions are becoming more attractive drivetrain options which reduces complexity while at the same time improving efficiency. It has been shown in [7] that medium-speed solutions can lead to improved annual energy yield.

Permanent magnet synchronous machines (PMSMs) have long been the preferred choice for wind generation systems.

PMSMs require no rotor winding and thus the physical size of the machine is reduced. Although this reduction in size can save on the total manufacturing costs, rare-earth permanent magnets are costly, and susceptible to large price variations and sourcing constraints [9]. Non-permanent magnet machines, such as wound-field machines, have generally lower overall material costs. Classical wound-field machines, such as the wound rotor synchronous machine (WRSM), have typically high losses associated with the brushed rotor windings as well as low power density [8]. On the other hand, the wound-field flux-switching machine (WF-FSM) is an example of a non-classical wound-field machine and it is characterised by high torque densities due to the flux modulation nature [10]. The WF-FSM is designed with the windings on the stator, which make them brushless among other things. Also, due to their large pole numbers for designs exhibiting high winding factors, as well as the so-called DC winding induced voltage pulsation, it is difficult to fix their voltages and frequency to the conventional grid, thus they are usually converter-operated [11], [12].

Meanwhile, interest in non-overlap windings has reignited due to the associated lower manufacturing costs, lower cogging torque and improved torque density [13]. They have been common in permanent magnet (PM) machines, but recent developments have focused on non-PM electric machines [14]. Overlap windings are characterized by a sinusoidal magnetomotive force (MMF) when the coils/slot/phase is high. This means that some MMF harmonic content is reduced, which translates to improved machine performance, but the winding manufacturing becomes more complex. Moreover, end-winding lengths are also very large, and the slot filling ability is low. By the adoption of non-overlap windings, many of the associated disadvantages of the distributed winding layout can be negated such as leading to a simple winding layout and reduced end-winding losses. The main disadvantage, however, is that the MMF spectrum of non-overlap windings consists of many sub- and higher-order harmonics. Harmonic reduction techniques based on phase-shift winding shows an improvement of the main harmonic, while the sub- and higher-order harmonics are largely diminished [15], [16].

The phase-shift winding WRSM, which exhibit flux-variation characteristic and reactive power compensation, typical in wound-field excited generators, is a very attractive option for direct grid-connected wind power generation [17]–[18]. The flux-variation characteristics allow for regulation of the phase voltage when the wind speed varies.

To this end, this study is a follow-up on the study discussed in [19], wherein the non-classical non-overlap phase shifting winding WRSM is designed, optimised and compared alongside the WF-FSM for 3 MW medium-speed wind power generation, for the first time. At such power levels and generator drivetrain, the attempt is to produce alternative wind generator technologies, which could compete with well-known PM variants in the niche utility scaling and drivetrain technology of future of wind power generation [2], [20], [21].

The intent of the current study is to experimentally evaluate the sub-scale performance of the phase-shift winding WRSM for direct-grid wind power generation as against the WF-FSM converter-fed wind generator drive, for the first time and with both machines designed in the medium-speed wind turbine operating regime. The study still highlights as already done in [19], the optimization and theoretic performance evaluation of both generator variants for medium-speed converter-fed systems at 3 MW power levels.

II. THEORETICAL DESIGN AND OPTIMISATION

The machines intended for the design optimisation are the three-phase 10 rotor poles/12 stator slots (10/12) WF-FSM design and the 16 poles/18 slots (16/18) WRSM, previously conceptualised and analysed in [12], [16], [22], [23] and [24]. A cross-sectional layout of each of the proposed machines and wind generator drivetrain are shown in Figures 1 and 2, respectively.

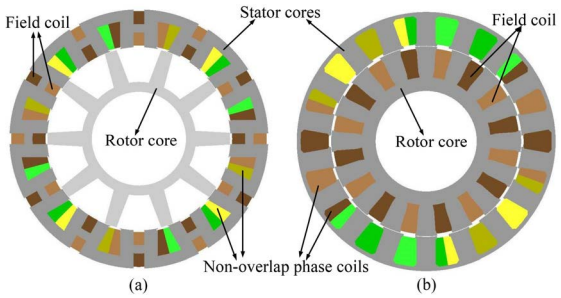

FIGURE 1. Cross-sections of non-overlap wound field machines: (a) 10/12 WF-FSM, and (b) 16/18 WRSM.

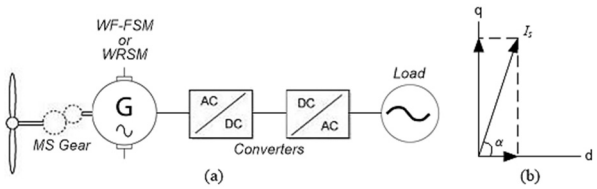

FIGURE 2. Proposed variable-speed wind energy system: (a) Sample geared medium-speed drivetrain, and (b) unvaried amplitude of generator supply current in dq vector frame.

The design optimisation conducted is to be based on a multi-objective multi-variable optimization algorithm – NSGA-II – originally proposed by authors in [25]. The highlight of this algorithm is in its ability to evolve multiple solutions of the competing objective parameters from a pool of both parental and offspring populations into a converged true Pareto-optimal front. It is important to emphasise that the accuracy of the optimisation is further linked to the tuning of specific parameter settings in line with the population size and the maximum number of generations. Hence, similar parameter settings are implemented at fixed population size of 20 and maximum iterations of 100, for both machines. The

optimisation problem is formulated as:

$$\text{minimise } F(\bar{x}) = \begin{bmatrix} M_A \\ \kappa_\delta \end{bmatrix} \tag{1}$$

$$\text{subject to } \begin{bmatrix} pF \\ P_{out} \\ \eta \end{bmatrix} \geq \begin{bmatrix} 0.8 \\ 3\ MW \\ 97\ \% \end{bmatrix} \tag{2}$$

where $F(\bar{x})$ is a vector of the objective parameter functions, comprising the total active mass (M_A) and per unit torque ripple (κ_δ) of the prescribed machines. These objectives have been nominated based on the following considerations:

- A lower active mass is adjudicated to ensure a better power/mass ratio. The lower the mass, the less material is required and in turn, the cheaper the machine and the lower the top-tower mass.
- Torque ripple is important for large electric machines, and especially for wind generator applications. Thus, very high torque ripple translates to vibrations in the machine, affecting its structural stability and causing excessive wear on the drivetrain components.
- The constraints placed on the efficiency and power factor are also important for the optimum performance of the proposed wind generator drivetrains. In [26], it is reported that a high efficiency/power factor unit reduces the kVA and costs of the drivetrain converters.

A number of design parameters are independently varied in both machines such as the phase current angle (α), armature current density (J), field current density (J_F), stack length (l_{st}), stator outer diameter (D_{out}), stator interior diameter (D_{in}) and rotor shaft diameter (D_{sh}), to mention a few. Based on the number of dimensional and non-dimensional variables, a total of 14 and 21 design variables were realised in the WF-FSM and WRSM designs, respectively. A reflection on some of the key base machine parameters conceived before the optimisation process, and the common design constants in both machines are presented in Table 1; the shaded columns report data captured for the optimal benchmark designs as later elucidated in Section III.

Dimensional and non-dimensional parametric optimisation is a common technique in modern electrical machine design and optimisation [27]. The choice of dimensional parameters such as stator outer and inner diameter because of the objective to reduce active mass, which we understand depends to a large extent on the conceived split ratios for wound-field machines [28]. In addition, the selection of non-dimensional parameters such as current density and current angle is because of tracking of performance variables such as torque and power factor, for which their optimal values yield tradeoffs [23].

The analysis algorithm as shown in Figure 3 is based on an in-house 2-D finite element analysis (FEA) package (SEMFEM) [29], which is then coupled to the optimiser (VisualDOC®) for the optimisation process as shown in Figure 4. SEMFEM is a fast and efficient program instituted for time-stepped static FEA simulation of electrical machine

TABLE 1. Initial and optimal display of selected design parameters.

	Parameters	WF-FSM		WRSM	
		Initial	Final	Initial	Final
Input design variables	D_{out} (m)	2.307	2.354	1.672	1.744
	D_{in} (m)	1.633	1.635	1.233	1.288
	l_{st} (m)	0.534	0.527	0.558	0.426
	D_{sh} (m)	0.840	0.892	0.653	0.790
	J (A/mm^2)	1.000	1.080	1.235	1.921
	J_F (A/mm^2)	4.908	4.999	4.718	4.763
	α (deg.)	49.745	89.870	76.762	88.610
Output variables	P_{out} (MW)	2.058	3.019	1.997	3.065
	pF	0.596	0.803	0.789	0.810
	η (%)	96.335	97.051	96.386	97.528
	κ_δ (%)	26.473	4.554	26.189	5.166
	M_{SA} (ton)	6.930	7.226	3.660	2.831
	M_{RA} (ton)	2.614	2.812	2.690	2.130
	M_A (ton)	9.544	10.038	6.350	4.961
	τ_e (kNm)	53.124	78.268	49.045	76.096
	Nm/kg	5.566	7.797	7.723	15.338
Constants	Ω_g (r/min)	360		375	
	f_e (Hz)	60		50	
	ρ_{Cu} (Ωm)	2.073×10^{-8}			
	g (mm)	3			
	K_{SP}	0.45			
	K_{SF}	0.45			

M_{SA} = stator active mass, M_{RA} = rotor active mass, τ_e = electromagnetic torque, $\boldsymbol{\Omega_g}$ = mechanical speed, f_e = frequency, ρ_{Cu} = copper resistivity, $\boldsymbol{g}$ = airgap length, K_{SP} = slot fill factor for phase windings, K_{SF}= slot fill factor for field windings

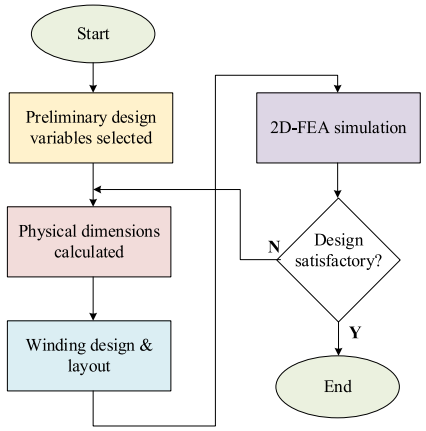

FIGURE 3. FEA design algorithm.

in 2-D. Based on the sample population size, the design variables are fed as input into the optimisation workflow shown in Figure 4, where the converge criteria is calculated and validated in FEA (Figure 3). The problem is looped continuously for convergence until the assigned generations are completed. The convergence to the true Pareto-optimal front in both machines is then adjudicated after the optimisation process, with the results and the benchmark performance comparison of both machines considered next.

III. OPTIMISATION RESULTS AND COMPARISON

Figures 5 and 6 show the optimum data of the Pareto-optimal front, as well as dispersion of the feasible solutions. Two optimal benchmark designs, one from each of the studied machines, earlier presented in Table 1, are identified in the

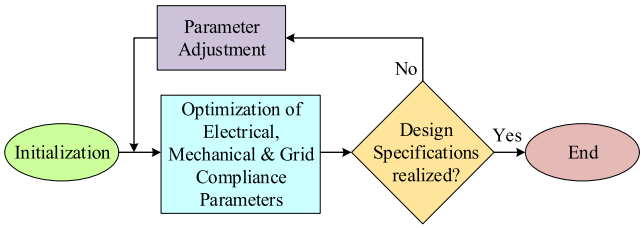

FIGURE 4. Optimisation framework.

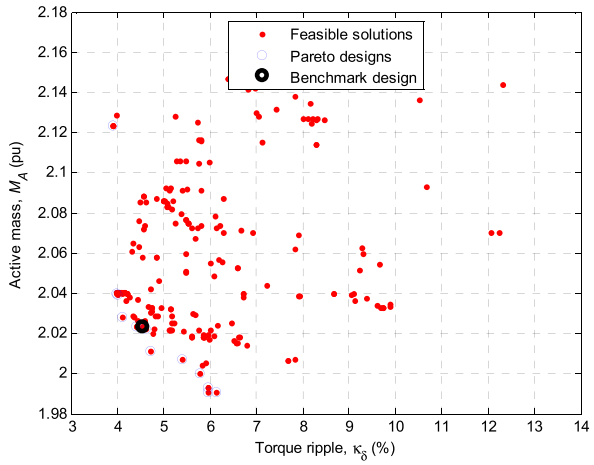

FIGURE 5. Pareto-optimal trends for 3 MW WF-FSM (1 pu = 4.961 ton).

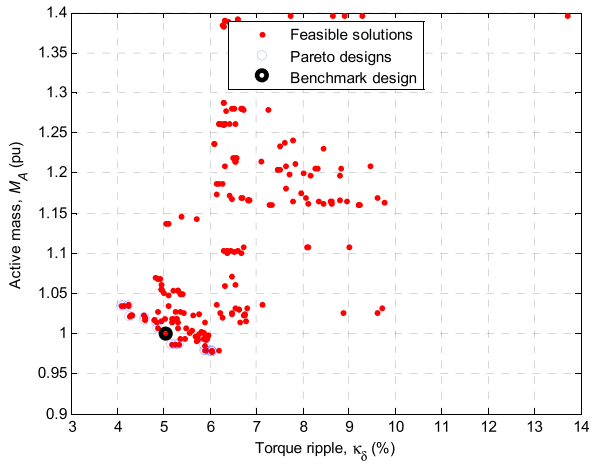

FIGURE 6. Pareto-optimal trends for 3 MW WRSM (1 pu = 4.961 ton).

figures. Observe that the per unit values of the active mass are based on the nominal value of the WRSM benchmark.

A tradeoff between the contrasted objectives (active mass and torque ripple) of both machines is portrayed in Figures 5 and 6, where increase in active mass results in torque ripple reduction, and vice versa. Also, the optimised torque ripple values are minimised to less than 5 %, especially for the WF-FSM which is notorious for high cogging torque due to its double salient structure. For the same torque ripple value, the active mass of the WF-FSM design is two times more than the WRSM design, although both seem to maintain the same torque per litre volume. The significantly higher mass of the WF-FSM is due to its inherent stator-mounted nature as both the phase and field windings housed on the stator, with the split and aspect ratio closely matched as shown in Table 2.

TABLE 2. Comparison of optimal split and aspect ratios.

Ratios	WF-FSM	WRSM	Deviation
$\Lambda_0\ (D_{in}/D_{out})$	0.694	0.738	5.962 %
$\kappa_L\ (l_{st}/D_{in})$	0.322	0.331	2.719 %

In Table 1, a further comparative data of the optimal benchmark designs, a higher phase current density is realised in the WRSM compared to the WF-FSM, due to larger slot filling areas of the phase windings. A linear interpolation of the optimisation dataset is undertaken of which the relationship between the stator outer diameter and the phase current density, as evinced in Figure 7, clearly shows an inverse relationship. The behaviour of D_{out} reflects the slot area allocation in such a way that the stator slots house only the phase windings in the WRSM, whereas for the WF-FSM, both the phase and field windings are collocated on the stator. Hence, one can see that as D_{out} decreases in the WRSM, J increases, whereas, for the WF-FSM, D_{out} increases with increase in J.

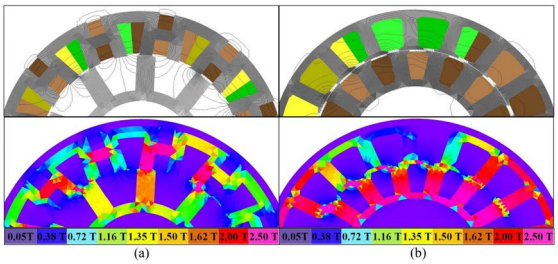

FIGURE 7. Optimal characteristics between stator outer diameter and phase current density.

The per unit reactance of the optimal benchmark machines are compared as shown in Table 3. Note that, X_d is reportedly greater than X_q because they are both evaluated at $\alpha = 70°$. Although with 12 % deviation, note that X_s can be approximately prescribed at 0.5 pu for both machines. This is due to similarities in constraints imposed on the airgap length, power factor, power and supply current of both machines. It is reported in [30] that such small values ($X_s \ll 1$ pu) would be profitable to the converters, in terms of reduced loss, KVA rating and cost. However, it can be argued that the fixed airgap length ($g = 3$ mm), assumed for both machines, influenced the low X_s value obtained in the WRSM more than the WF-FSM considering the smaller stator outer diameter of the former [31].

Figure 8 maps the 2-D FEA flux line distributions and flux densities for the optimal machine benchmarks at rated load conditions. The peak airgap flux density is observed at 2.84 T and 2.52 T in the WF-FSM and WRSM, respectively. The

TABLE 3. Comparison of reactances for benchmark wound-field machines.

Parameters	WF-FSM	WRSM
X_d (pu)	0.491	0.394
X_q (pu)	0.506	0.482
X_s (pu)	0.498	0.438
V_T (V)	639.488	634.275
$I_{s\,(\mathrm{RMS})}$ (kA)	3.296	3.266

X_d = d-axis reactance, X_q = q-axis reactance, X_s = synchronous reactance, V_T = line (terminal) voltage, $I_{s\,(\mathrm{RMS})}$ = RMS supply current

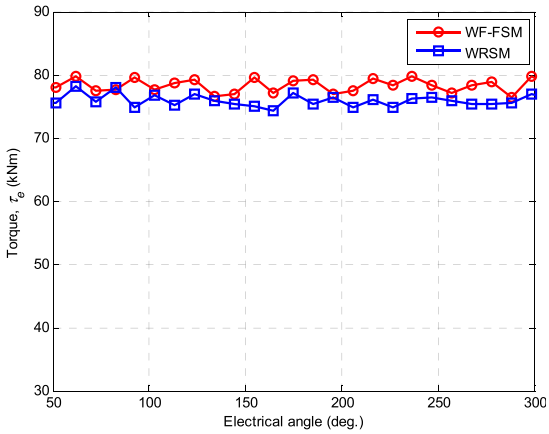

FIGURE 8. 2-D FEA field lines and flux densities for 3 MW machines under rated conditions: (a) WF-FSM, and (b) WRSM.

higher peak airgap flux density recorded in the WF-FSM is due to cross-coupling effects [23].

The higher-level saturation in the rotor core of the WRSM compared to the WF-FSM is due to very high ampere-turns of its rotor field windings, as elucidated by the optimum current density values in Table 1. Such oversaturation of the rotor core has been attributed to high torque ripple effects in WRSMs [32]. The issue could be addressed by decreasing the slot fill factor of the field windings, but at the expense of declining the optimal torque density of the WRSM. In Figure 9, the 2-D FEA predicted torque waveforms of the optimal benchmarks under rated load conditions are shown.

An effective comparison on the studied machines has been undertaken as shown in Table 4. A substantial reduction in size and mass of the proposed WRSM wind generator for the same power level and performance constraints as that of the WF-FSM has been observed. However, other factors need to be properly weighed such as fabrication and maintenance costs, which should be lower for the WF-FSM. But more importantly, the non-utilisation of PMs has been fully demonstrated in the studied wound-field machine topologies.

IV. EXPERIMENTAL DEMONSTRATION

In this section, sub-scaled prototypes of the WF-FSM [28] and the phase-shifted winding WRSM are demonstrated [24]. The machine design and rated parameters of both prototypes are presented in Table 5. As earlier indicated, the WF-FSM is tested as a converter-fed generator while the WRSM is tested as a direct grid-connected generator. Figure 10 shows the test rig for the 10 kW WF-FSM generator prototype, while Figure 11 shows that of the 3 kW WRSM. Due to voltage limitation of the power converters, measurements conducted for the WF-FSM were done at half the prescribed rated conditions.

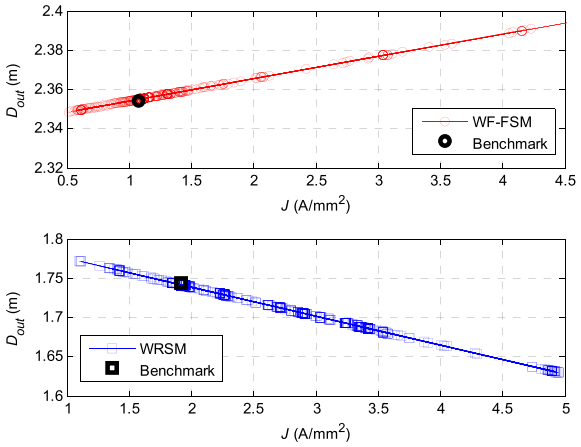

FIGURE 9. Electromagnetic torque waveforms of 3 MW optimal wind generator benchmarks under rated conditions.

TABLE 4. Effective performance comparison of the studied 3 MW non-overlap wound-field wind generators.

Design issue	WF-FSM	WRSM
Mass saving	Low	High
Field excitation	Cheap	Expensive
Simple and robust rotor	Yes	No
Simple stator	No	Yes
Temperature management	Extrinsic	Intrinsic
Active copper slot areas	Small	Large
Torque density	Low	High
Saturation	Light	Heavy
Converter	Yes	Yes
Gearbox	Yes	Yes
Reliability	High	Low
Synchronous reactance	Low	Low
Airgap length	Underestimated	Overestimated

TABLE 5. Main parameters for non-overlap winding machine prototypes.

Parameters	WF-FSM	WRSM
Stator outer diameter (mm)	600	260
Rotor outer diameter (mm)	414.7	203.6
Stack length (mm)	104	125
Air gap thickness (mm)	0.7	0.45
Number of rotor poles	10	16
Number of stator slots	12	18
Rated speed (r/min)	360	375
Rated frequency (Hz)	60	50
Rated phase current (A)	9.8	4.86
Rated field current (A)	15.6	5.00
Rated line voltage (V)	590	350
Rated terminal power (kW)	10	3

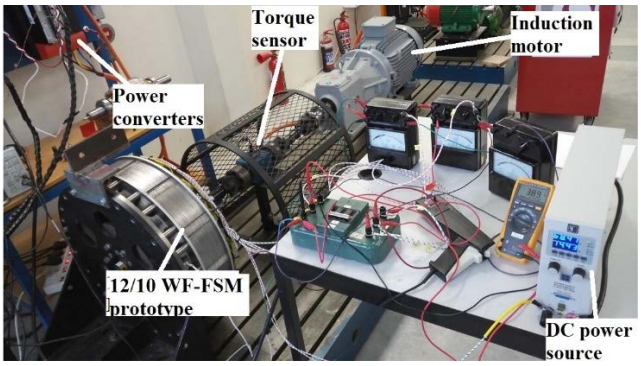

FIGURE 10. Test rig 10 kW 10/12 pole/slot WF-FSM generator prototype.

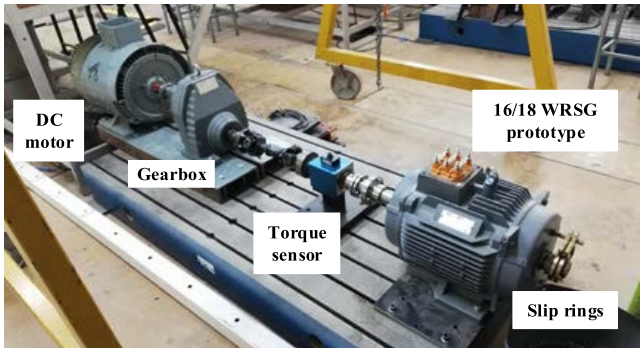

FIGURE 11. Test rig for 3 kW 16/18 pole/slot WRSM generator prototype.

The comparison of the no-load and rated torque profiles, as well as voltage regulation, between FEA and measurement for both prototype machines, is shown in Table 6. The disagreement between simulated and measured results is due to manufacturing defects on the prototypes as well as unsolicited fringing effects in the FEA models, especially for the WF-FSM. The finite element analysis process cannot fully account for the end leakages, especially with errors during the manufacturing process. The improper estimation of the end leakages means that the actual phase winding inductances are not in line with the theoretical values. This is also compounded by constraints on the fill factors while mounting the windings.

TABLE 6. Comparison of torque profiles and voltage regulation for non-overlap winding machine prototypes.

	WF-FSM		WRSM	
	FEA	Test	FEA	Test
Cogging torque (%)	10.6	5.0	7.3	5.4
Torque ripple (%)	10.2	14.1	6.7	8.2
Average torque (Nm)	244.5	219.9	83.7	81.8
Voltage regulation (%)	9.2	19.2	4.5	5.6
Core loss (W)	211.4	249.3	60.8	62.6

In Figures 12 and 13, the generator efficiency is evaluated for the WF-FSM and WRSM, respectively, under rated phase current and varying load conditions of the field current. It is clear from both figures that more power can be generated as

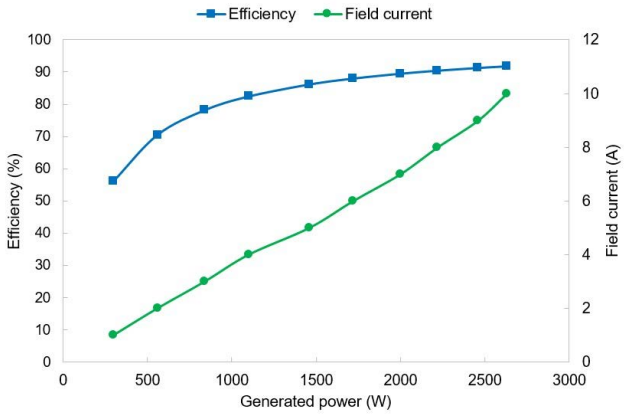

FIGURE 12. Efficiency and field current versus generated power tests on the converter-fed WF-FSM generator prototype, $I_{Load} = 9.2$ A and 180 r/min.

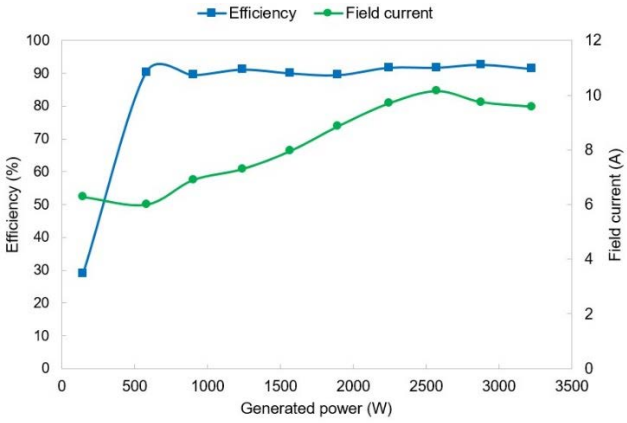

FIGURE 13. Efficiency and field current versus generated power tests on the grid-connected WRSM phase-shift winding generator prototype, $I_{Load} = 492$ A and 375 r/min.

field current is increased, which can be easily aligned to the varying wind resource for optimum power capability. Additionally, it can be noted that, unlike the WF-FSM converter-fed generator, the WRSM direct grid-connected generator offers higher efficiency performance across a diverse operating load regime. No doubt, the wider improved efficiency range of the WRSM is due to a better voltage regulation recorded in Table 6, since the generator terminal voltage is tied to the grid voltage.

Also, the experimented steady-state heat maps for the WF-FSM at different temperature hotspots, as well as the thermal test heat runs under short-circuit condition are presented in Figures 14 and 15. These hotspots are prioritized by careful inspection of the broad surrounding of the machine's stator under prolonged short-circuit tests as captured in Figure 16 using a digital thermographic camera. The different hotspots show the rapid thermal build up in parts of the field coils compared to the armature coils. This is due to the intrinsic positioning and higher current density of the former, although the performance of the machine is not threatened as

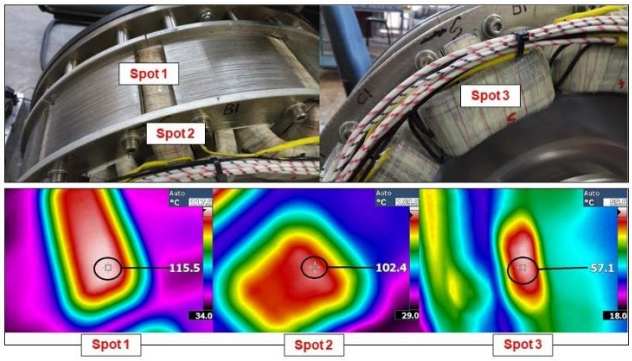

FIGURE 14. Key thermal hotspots for WF-FSM prototype.

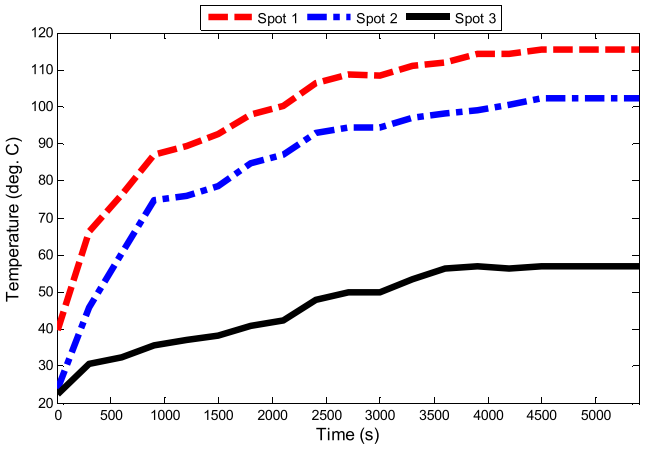

FIGURE 15. Heat runs under short-circuit condition for WF-FSM prototype.

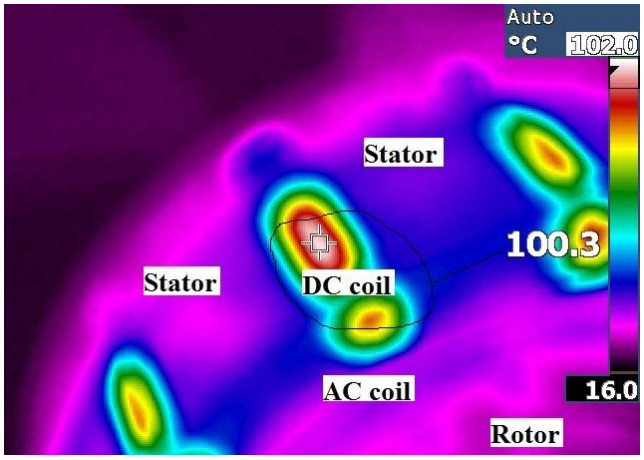

FIGURE 16. Snapshot displaying very low–profile thermal activity on the stator body and thermal concentration on the coils of the WF-FSM prototype.

the risk of demagnetization is zero. Regarding the WRSM, only the temperature rise over time of the prototype casing under rated field and phase current is shown in Figure 17. This is because, unlike the WF-FSM prototype, the WRSM prototype is built within an enclosed frame.

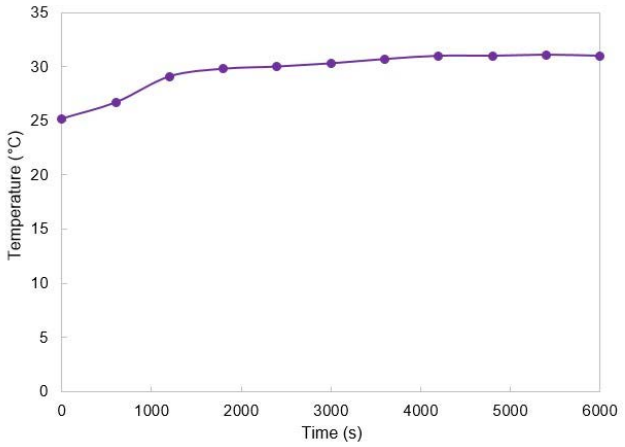

FIGURE 17. Heat run under full load condition for the WRSM prototype.

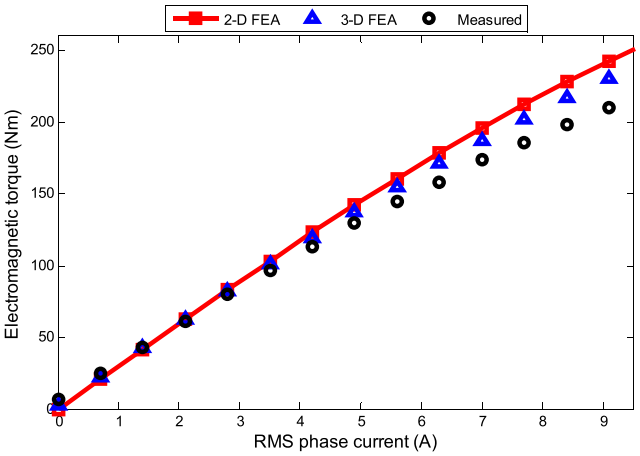

FIGURE 18. FEA predicted and measure torque under varying load current for the WF-FSM prototype ($I_F = 15.6$ A).

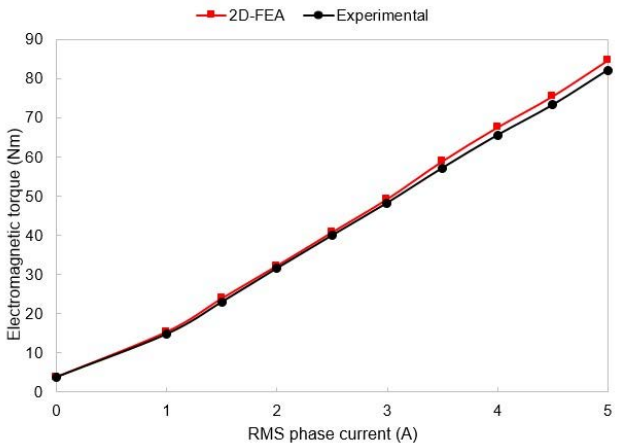

FIGURE 19. FEA predicted and measure torque under varying load current for the WF-FSM prototype ($I_F = 5$ A).

Lastly, the electromagnetic torque versus load current profiles of the WF-FSM and WRSM are provided in Figures 18 and 19, respectively. The comparison between

FEA and experiments show good match, although due to its stator-mounted nature, some notable discrepancy is observed for the WF-FSM due to increased saturation with increasing load current, as well as manufacturing defects.

V. CONCLUSION

In this study, finite element analysis-based optimisation on large-scale and experimentation on sub-scaled power levels of two distinct non-conventional, non-overlap wound-field machines have been investigated for medium-speed wind generator drivetrains in converter-fed versus direct grid-connected modes, for the first time. The comparison is based on 10/12 pole/slots wound-field flux switching machine (WF-FSM) and 16/18 wound-rotor synchronous machine (WRSM). Based on benchmark design candidates from the global optimisation of both machines at large-scale power levels, the torque per mass of the WF-FSM is observed to be half of that of the WRSM subjected under the same torque per litre. The optimal mass discrepancy in both machines could be attributed to the evolution of closely matched optimal split and aspect ratios. In terms of sub-scaled experimentation, the WF-FSM was tested in converter-output mode while the WRSM was tested in direct grid-connected mode. The experimental results clearly show that both generators easily vary their generated output power to match with varying wind resource, but the latter can offer an improved efficiency range since the generator terminal voltage is better regulated.

REFERENCES

[1] REN21. (2020). *Renewables 2020 Global Status Report (Paris: REN21 Secretariat)*. [Online]. Available: https://www.ren21.net/gsr
[2] S. K. Moore, "Rough seas for the superconducting wind turbine: To keep offshore turbines light, engineers look beyond superconductors to a new permanent-magnet tech," *IEEE Spectr.*, vol. 55, no. 8, pp. 32–39, Aug. 2018.
[3] T. Balachandran, A. Yoon, D. Lee, J. Xiao, and K. S. Haran, "Ultrahigh-field, high-efficiency superconducting machines for offshore wind turbines," *IEEE Trans. Magn.*, vol. 58, no. 2, pp. 1–5, Feb. 2022.
[4] H. Chen, Y. Zuo, K. T. Chau, W. Zhao, and C. H. T. Lee, "Modern electric machines and drives for wind power generation: A review of opportunities and challenges," *IET Renew. Power Gener.*, vol. 15, no. 9, pp. 1864–1887, 2021.
[5] P. H. Jensen, T. Chaviaropoulos, and A. Natarajan, "LCOE reduction for the next generation offshore wind turbines," INWIND.EU Project, Tech. Univ. Denmark, Lyngby, Denmark, Tech. Rep., Oct. 2017.
[6] D. K. K. Padinharu, G.-J. Li, Z.-Q. Zhu, R. Clark, A. Thomas, Z. Azar, and A. Duke, "Permanent magnet Vernier machines for direct-drive offshore wind power: Benefits and challenges," *IEEE Access*, vol. 10, pp. 20652–20668, 2022.
[7] E. De Vries, *Electrical Drives for Direct Drive Renewable Energy Systems*. Sawston, U.K.: Woodhead Publishing, 2013.
[8] C. C. Pavel, R. Lacal-Arántegui, A. Marmier, D. Schüler, E. Tzimas, M. Buchert, W. Jenseit, and D. Blagoeva, "Substitution strategies for reducing the use of rare earths in wind turbines," *Resour. Policy*, vol. 52, pp. 349–357, Jun. 2017.
[9] D. Fallows, S. Nuzzo, and M. Galea, "An evaluation of exciterless topologies for medium power wound-field synchronous generators," in *Proc. 10th Int. Conf. Power Electron., Mach. Drives (PEMD)*, 2021, pp. 116–121.
[10] D. Li, R. Qu, and J. Li, "Topologies and analysis of flux-modulation machines," in *Proc. IEEE Energy Convers. Congr. Expo. (ECCE)*, Montreal, QC, Canada, Sep. 2015, pp. 2153–2160.
[11] Z. Wu, Z.-Q. Zhu, C. Wang, J.-C. Mipo, S. Personnaz, and P. Farah, "Analysis and reduction of on-load DC winding induced voltage in wound field switched flux machines," *IEEE Trans. Ind. Electron.*, vol. 67, no. 4, pp. 2655–2666, Apr. 2020, doi: 10.1109/TIE.2019.2912779.
[12] U. B. Akuru and M. J. Kamper, "Formulation and multiobjective design optimization of wound-field flux switching machines for wind energy drives," *IEEE Trans. Ind. Electron.*, vol. 65, no. 2, pp. 1828–1836, Feb. 2018.
[13] G. Dajaku, S. Spas, X. Dajaku, and D. Gerling, "An improved fractional slot concentrated winding for low-poles induction machines," in *Proc. 19th Int. Conf. Electr. Mach. (ICEM)*, Lausanne, Switzerland, Sep. 2016, pp. 116–121.
[14] S. Lengsfeld, J. Grundmann, M. Oomen, C. Vargas-Llanos, B. Ponick, and M. Jung, "Comparing armature windings for a 10 MW fully superconducting synchronous wind turbine generator," in *Proc. 12th Int. Conf. Power, Energy Electr. Eng. (CPEEE)*, Feb. 2022, pp. 49–53.
[15] Z. Wu, Z. Q. Zhu, and C. Wang, "Reduction of on-load DC winding-induced voltage in partitioned stator wound field switched flux machines by dual three-phase armature winding," *IEEE Trans. Ind. Electron.*, vol. 69, no. 6, pp. 5409–5420, Jun. 2022.
[16] K. S. Garner and M. J. Kamper, "Reducing MMF harmonics and core loss effect of non-overlap winding wound rotor synchronous machine (WRSM)," in *Proc. IEEE Energy Convers. Congr. Expo. (ECCE)*, Cincinnati, OH, USA, Oct. 2017, pp. 1850–1856.
[17] H. M. Yassin, R. R. Abdel-Wahab, and H. H. Hanafy, "Active and reactive power control for dual excited synchronous generator in wind applications," *IEEE Access*, vol. 10, pp. 29172–29182, 2022.
[18] J. H. Giliomee and M. J. Kamper, "Maximum power point field control of direct DC grid-connected wound rotor synchronous wind generator system," in *Proc. 30th Southern Afr. Univ. Power Eng. Conf. (SAUPEC)*, Jan. 2022, pp. 1–6.
[19] U. B. Akuru, K. S. Garner, and M. J. Kamper, "Design optimisation and comparison of large-scale non-overlap wound-field machines," in *Proc. XIII Int. Conf. Electr. Mach. (ICEM)*, Alexandroupoli, Greece, Sep. 2018, pp. 2117–2122.
[20] S. Watson *et al.*, "Future emerging technologies in the wind power sector: A European perspective," *Renew. Sustain. Energy Rev.*, vol. 113, Oct. 2019, Art. no. 109270.
[21] G. van de Kaa, M. van Ek, L. M. Kamp, and J. Rezaei, "Wind turbine technology battles: Gearbox versus direct drive–opening up the black box of technology characteristics," *Technol. Forecasting Social Change*, vol. 153, Apr. 2020, Art. no. 119933.
[22] K. S. Garner and M. J. Kamper, "Performance comparison of large-scale design-optimised non-overlap and overlap winding wound rotor synchronous generators," in *Proc. IEEE Energy Convers. Congr. Expo. (ECCE)*, Oct. 2021, pp. 4234–4239.
[23] M. Mabhula, U. B. Akuru, and M. J. Kamper, "Cross-coupling inductance parameter estimation for more accurate performance evaluation of wound-field flux modulation machines," *Electronics*, vol. 9, no. 11, p. 1748, Oct. 2020.
[24] K. S. Garner, M. J. Kamper, and A. T. Loubser, "Performance evaluation of harmonic reduced non-overlap winding wound rotor synchronous machine," *Energies*, vol. 14, no. 22, p. 7501, Nov. 2021.
[25] K. Deb, A. Pratap, S. Agarwal, and T. Meyarivan, "A fast and elitist multiobjective genetic algorithm: NSGA-II," *IEEE Trans. Evol. Comput.*, vol. 6, no. 2, pp. 182–197, Apr. 2002.
[26] Y. Wang, J. Sun, Z. Zou, Z. Wang, and K. T. Chau, "Design and analysis of a HTS flux-switching machine for wind energy conversion," *IEEE Trans. Appl. Supercond.*, vol. 23, no. 3, Jun. 2013, Art. no. 5000904.
[27] G. Bramerdorfer, J. A. Tapia, J. J. Pyrhönen, and A. Cavagnino, "Modern electrical machine design optimization: Techniques, trends, and best practices," *IEEE Trans. Ind. Electron.*, vol. 65, no. 10, pp. 7672–7684, Oct. 2018.
[28] U. B. Akuru and M. J. Kamper, "Intriguing behavioral characteristics of rare-earth-free flux switching wind generators at small- and large-scale power levels," *IEEE Trans. Ind. Appl.*, vol. 54, no. 6, pp. 5772–5782, Nov. 2018.
[29] *SEMFEM Documentation*. Accessed: Dec. 2021. [Online]. Available: https://www0.sun.ac.za/semfem/index.html
[30] I. Boldea, L. Tutelea, and F. Blaabjerg, "High power wind generator designs with less or no PMs: An overview," in *Proc. 17th Int. Conf. Electr. Mach. Syst. (ICEMS)*, Hangzhou, China, Oct. 2014, pp. 1–14.
[31] E. L. Engevik, T. E. Hestengen, M. Valavi, and A. Nysveen, "Effects of lifting reactance requirements on the optimal design of converter-fed synchronous hydrogenerators," in *Proc. IEEE Int. Electr. Mach. Drives Conf. (IEMDC)*, Miami, FL, USA, May 2017, pp. 1–8.

KAREN S. GARNER (Member, IEEE) was born in Cape Town, South Africa, in October 1985. She received the B.Eng. degree in electrical and electronic engineering from Stellenbosch University, in 2007, the M.Eng. degree in electrical engineering from North-West University, in 2015, and the Ph.D. degree in electrical engineering from Stellenbosch University, in December 2021. She worked as an Electrical Engineer in the petrochemical industry, from 2008 to 2016, completing multibillion-dollar projects from concept to construction. She is currently working as a Lecturer with Stellenbosch University. She is registered as a Professional Engineer in South Africa and is supported by the South African National Research Foundation. Her research interests include novel electric machines, renewable energy, and power transmission. She is a member of SAIEE.

UDOCHUKWU B. AKURU (Senior Member, IEEE) received the B.Eng. and M.Eng. degrees from the University of Nigeria, Nsukka, in August 2008 and June 2013, respectively, and the Ph.D. degree in electrical engineering from Stellenbosch University, South Africa, in December 2017.

He held a Postdoctoral Research Fellowship at Stellenbosch University, between 2018 and 2020. He is currently a Senior Lecturer with the Tshwane University of Technology, South Africa. He has published widely in journals and conference outlets, and also acts as a reviewer of IEEE TRANSACTIONS and conferences. His main research interests include electrical machines design, electrical power, and renewable energy.

Dr. Akuru is a Registered Engineer of the Council for the Regulation of Engineering in Nigeria (COREN); a Senior Member of SAIEE; a South African National Research Foundation (NRF)-Rated Researcher; and a volunteer to various societies, committees, and groups, such as IEEE IAS EMC and IEEE IES EMTC. He was a recipient of several grants and awards, including the prestigious Jorma Luomi Student Forum Award at the 2018 International Conference on Electrical Machines (ICEM) and the 2020 TWAS-DFG Research Fellowship.

MAARTEN J. KAMPER (Senior Member, IEEE) received the M.Sc. (Eng.) and Ph.D. degrees from Stellenbosch University, Stellenbosch, South Africa, in 1987 and 1996, respectively.

He has been an Academic Staff of the Department of Electrical and Electronic Engineering, Stellenbosch University, since 1989, where he is currently a Professor of electrical machines and drives. His research interests include computer-aided design and control of reluctance, permanent magnet, and inductance machine drives. He is a South African National Research Foundation (NRF)-Rated Researcher and a Registered Professional Engineer in South Africa.